Enhanced quasi-distributed accelerometer array based on φ-OTDR and ultra-weak fiber Bragg grating

Hua Zheng, Huan Wu, Chern Yang Leong, Yuyao Wang, Xinliang Shen, Zheng Fang, Xin Cheng, Jingxian Cui, Dingjiong Ma, Yun Miao, Li Zhou, Min Yan, Jie Sun, Hwa-Yaw Tam, Xiaoli Ding, Chao Lu,

***Abstract*—We propose and experimentally demonstrate an enhanced quasi-distributed accelerometer array based on *φ*-OTDR and ultra-weak fiber Bragg grating (UWFBG). By utilizing a transducer cylinder, the vibration can be easily converted to an axial strain of the sensing fiber, which enables a high sensitivity in vibration measurement. Furthermore, an UWFBG array that contains backscattering enhanced points along the fiber is employed to improve the signal-to-noise ratio (SNR). Consequently, quasi-distributed vibration sensing with a resolution of 0.03 g, and a flat sensitivity of 1.4 rad/g in a frequency range from 50 to 800 Hz is realized over 500-m long UWFBG. The proposed sensing system offers high sensing sensitivity, large multiplexing capacity, and anti-interference fading, which can be applied for structural health monitoring of large buildings and machinery.**

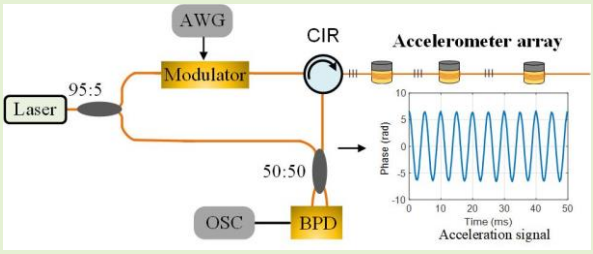

***Index Terms*—Phase-Sensitive Optical Time Domain Reflectometry (*φ*-OTDR), distributed optical fiber sensing, accelerometer.**

I. Introduction

An accelerometer is an inertial sensor that can measure vibrations induced by external forces which may vary in magnitude, direction, and frequency [1–3]. Traditional electrical accelerometers are mainly based on piezoelectric effect, piezoresistive effect, and capacitance change induced by a vibration [4–6]. Though these sensors are mature and have been applied in many industrial applications, in some harsh environments such as the coal mining industry, oil/gas industry, and underground environments, these electrical accelerometers are unsuitable due to their susceptibility to electromagnetic interferences (EMI), difficulties in providing power supply and unreliable data transmission over a long distance [7,8]. However, high-performance accelerometers with high sensitivity, large measurement range, and wide frequency response are in demand in these scenarios. Optical fiber accelerometers are good substitutes in these harsh environments. Inheriting the characteristics of optical fiber, accelerometers based on optical fiber are immune to EMI, support high-speed data transmission over a long distance, and do not need power supply to the sensors [9,10].

Optical fiber sensors can be broadly classified into two categories, single-point sensors, and distributed sensors. In the past decades, different kinds of single-point or quasi-distributed optical fiber accelerometers have been proposed, including wavelength-demodulation sensors utilizing fiber Bragg grating (FBG) [1], [2] and phase-demodulation sensors based on fiber interferometers including Michelson interferometer [3], [4], Fabry-Perot interferometer [5], and Sagnac interferometer [6]–[8]. The sensitivity of these optical fiber accelerometers varies from a few pm/g to hundreds of pm/g, and the operational frequency range can reach kHz. Meanwhile distributed acoustic sensors (DAS) based on phase-sensitive optical time-domain reflectometry (φ-OTDR) attracted much attention from both the industry and academia in recent years [9]–[18]. They possess the characteristics of both long-distance measurement and high

This work was supported by Postdoc Matching Fund Scheme of the Hong Kong Polytechnic University(1-W23E), RGC GRF project (15209919), ITC Project K-BBY1. The authors would also like to acknowledge the support from Theory Lab, Central Research Institute, 2012 Labs, Huawei Technology Co. Ltd. *(Corresponding author: Huan Wu.)*

Hua Zheng, Huan Wu, Yuyao Wang, Xinliang Shen, Zheng Fang and Chao Lu are with the Department of Electronic and Information Engineering, The Hong Kong Polytechnic University, Hong Kong SAR.(e-mail: hkpolyu.wu@polyu.edu.hk)

Chern Yang Leong, Xin Cheng, Jingxian Cui and Hwa-Yaw Tam are with the Department of Electrical Engineering, The Hong Kong Polytechnic University, Hong Kong SAR.

Xiaoli Ding is with the Department of Land Surveying and Geo-informatics, The Hong Kong Polytechnic University, Hong Kong SAR.

Dingjiong Ma, Min Yan and Jie Sun are with Theory Lab, Central Research Institute, 2012 Labs, Huawei Technology Co. Ltd., Hong Kong, China.

Yun Miao, Li Zhou are with Theory Lab, Central Research Institute, 2012 Labs, Huawei Technology Co. Ltd., Shanghai,P.R. China.

spatial resolution distributed sensing. Compared with single-point optical fiber sensors, DAS only needs one interrogator to demodulate the vibration signals from hundreds even thousands of sensing positions. However, DAS is only sensitive to the axial strain changes, which makes the coupling between vibration and axial strain of fiber critically important. To solve this problem, an accelerometer array based on dual-pulse phase-sensitive OTDR was proposed in 2018 [19]. By coiling a single-mode fiber (SMF) on a transducer, inertial force generates strain on the fiber, which can be converted to the phase shift of Rayleigh backscattering (RBS). An accelerometer array with a sensitivity of ~36 rad/g was demonstrated. However, the RBS is very weak in SMF (Rayleigh scattering coefficient is approximately 5×10^{-8}/m at 1550 nm [20]). Therefore, RBS traces have a limited signal-to-noise ratio (SNR), which will eventually affect the performance of the accelerometer array.

In this paper, we propose to improve the performances of the accelerometer array by utilizing ultra-weak fiber Bragg grating (UWFBG) in a heterodyne detection DAS system. By embedding reflecting points into SMF, the reflectivity can be improved to 0.01% (-40dB), which is around 15 dB higher than the Rayleigh backscattering in a standard SMF. Therefore, the overall performance of an accelerometer in terms of sensitivity, signal fidelity, and fading probability can be greatly improved. An interference fading free accelerometer array with a resolution of 0.03 g, sensitivity of 1.4 rad/g, and dynamic range of 280 g was demonstrated over a 500-m long UWFBG sensing fiber. Compared with the SMF accelerometer, an SNR enhancement of 10.4 dB is achieved by using UWFBG. The proposed sensing system offered a promising solution for quasi-distributed vibration sensing with high sensing sensitivity, large multiplexing capacity, interference fading-free measurement at the same time.

II. Principle

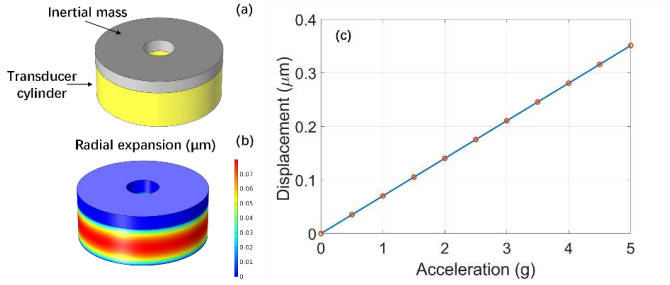

Fig. 1. (a) Schematic figure of the transducer. (b) Simulated radial expansion of the polyurethane when 1 g acceleration is applied. (c) Calculated radial expansion as a function of acceleration of up to 5 g.

The schematic diagram of the designed transducer of the optical fiber accelerometer is illustrated in Fig. 1(a). A stainless-steel cylinder (37 grams) with an inner diameter of 1 cm, outer diameter of 4 cm, and height of 0.4 cm is used as the inertial mass. The transducer cylinder is made of polyurethane and its height is 1.2 cm (the inner diameter and outer diameter are the same as inertial mass). The Young's modulus of polyurethane is 20 Mpa and its Poisson ratio is 0.42. When the acceleration is changed, the inertial mass will compress or decompress the transducer cylinder as the inertial mass move toward and away from the transducer cylinder, respectively, and subsequently induces expansion and reduction of the transducer cylinder in the radial direction. The designed compact structure can work in tight spaces, which is very suitable for applications including conveyor and mine monitoring. Fig. 1(b) shows the simulated radial expansion of the transducer cylinder when an acceleration of 1 g is applied by using finite element software. An expansion of 0.07 μm can be observed at the central section of the transducer cylinder. The relationship between the acceleration and the radial expansion is also calculated as shown in Fig. 1(c). It can be observed that the displacement changes linearly with the acceleration. When a section of fiber is wrapped on the transducer cylinder, the radial expansion will change the fiber length and induce a phase shift. Consequently, the acceleration phase sensitivity of the sensor in the flat response region can be expressed as:

$$S = \frac{\Delta\varphi}{a} = 4\pi\frac{2\pi n\Delta dN\eta}{\lambda a} \tag{1}$$

where $\Delta\varphi$ is the phase shift, a is the acceleration, n is the refractive index of fiber, Δd is the radial expansion, N is the number of fiber turns around the cylinder, λ is the wavelength of laser source, and η is the length conversion coefficient, since Young's modulus of polyurethane and fiber coating is much smaller than that of the fused silica, the radial expansion of the polyurethane cannot be fully converted to the length change of the optical fiber. Assuming the wrapped fiber is between ith and (i+1)th UWFBG, the backscattered light of the two UWFBG can be expressed as:

$$E_i = E_0\sqrt{r}\cos(\omega t + \varphi_i) \tag{2}$$

$$E_{i+1} = E_0\sqrt{r}\cos(\omega t + \varphi_{i+1}) \tag{3}$$

where E_0 is the electric field of the incident light, r is the reflectivity of UWFBG, φ_i and φ_{i+1} are the initial phases. After beating with the local oscillator (LO), the intensity of the output beating photocurrent can be expressed as:

$$I_i(t) \propto 2\sqrt{r}E_0E_L\cos(\Delta\omega t + \varphi_i) \tag{4}$$

$$I_{i+1}(t) \propto 2\sqrt{r}E_0E_L\cos(\Delta\omega t + \varphi_{i+1}) \tag{5}$$

where E_L is the electric field of LO, $\Delta\omega$ is the frequency shift induced by AOM. By using an in-phase and quadrature (IQ) algorithm, the phase shift of ith and (i+1)th UWFBG can be demodulated, and the measured acceleration can be expressed as:

$$a = \frac{\varphi_{i+1} - \varphi_i}{S} \tag{6}$$

III. Experimental Setup

The experimental setup of the DAS system is shown in Fig. 2. A narrow-linewidth laser (Connect CoSF-SC-1550-M) with 5kHz linewidth is employed as the coherent optical source. Its output is +3 dBm with the central wavelength at 1550.1 nm. The lightwave is split by a 95:5 coupler into two parts. The 95% lightwave is frequency shifted by an acoustic-optic modulator (AOM) and pulsed by a semiconductor optical amplifier (SOA). The electrical pulse is generated by an arbitrary waveform generator (AWG, BK Precision 4065). The pulse width is 40 ns with a repetition rate of 100kHz. An erbium-doped fiber

amplifier (EDFA, Amonics AEDFA-18-M-FA) is used to boost the power of the optical pulses. The amplified spontaneous emission (ASE) noise is filtered out by an optical bandpass filter with 100 GHz bandwidth. Then the optical pulses are launched into the fiber-under-test (FUT). The FUT is 160 m G.652 SMF connected with 500 m UWFBG. The backscattering is further amplified by another EDFA and followed by another 100 GHz bandpass optical filter. Finally, the backscattering is combined with the optical local oscillator from the lower branch and launched into a balanced photo-detector (BPD, Thorlabs PDB465C) with a bandwidth of 200 MHz. The electrical signal from the BPD is then sampled by an oscilloscope (Keysight MSOS404A) with a sample rate of 1 GS/s and the collected data are sent to a computer for further processing.

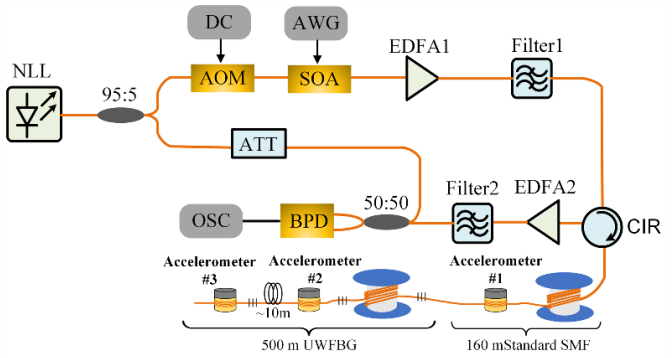

Fig. 2. Experimental setup of the DAS.NLL: narrow-linewidth laser; AOM: acoustic-optic modulator; SOA: semiconductor optical amplifier; AWG: arbitrary waveform generator; EDFA: erbium-doped fiber amplifier; ATT: attenuator; CIR: circulator; BPD: balanced photo-detector; OSC: oscilloscope.

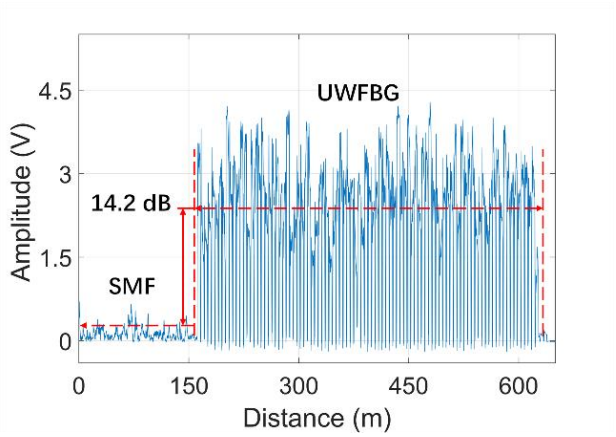

Fig. 3. Measured backscattering trace of the FUT using direct detection DAS.

The FUT is first characterized by using a direct detection DAS with a 16 ns probe pulse, the measured backscattering trace is shown in Fig. 3. Due to the interference superposition between multiple scatters within one pulse width, the trace of Rayleigh scattering in SMF shows a random jagged profile. In the destructive interference point, the intensity is extremely low, which leads to a fading phenomenon in phase demodulation. Compared with SMF, the UWFBG shows a 14.2 dB stronger backscattering coefficient, which can greatly improve the SNR of backscattered light and eliminate interference fading. The spacing interval between adjacent UWFBG is 5m, which is equal to the spatial resolution of the system. The 3 dB bandwidth of UWFBG is 5 nm, central wavelength is 1549 nm and the grating length is 10 mm which enables a stable reflectivity over -40 ℃~90 ℃.

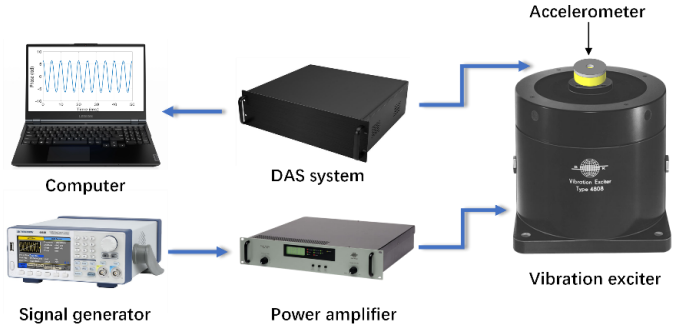

Fig. 4. Experimental setup for the evaluation of the accelerometer.

To evaluate the performance of the optical fiber accelerometer, a permanent magnet vibration exciter (Bruel & Kjaer type 4808) is used to provide the acceleration as shown in Fig. 4. The vibration exciter can provide an acceleration up to 50 g and vibrations with a frequency below 2.5 kHz. In order to monitor in real-time the acceleration value of the vibration exciter, a piezoelectric accelerometer (Bruel & Kjaer type 8305) is also attached under the shaker platform for reference.

IV. Experimental Results and Discussions

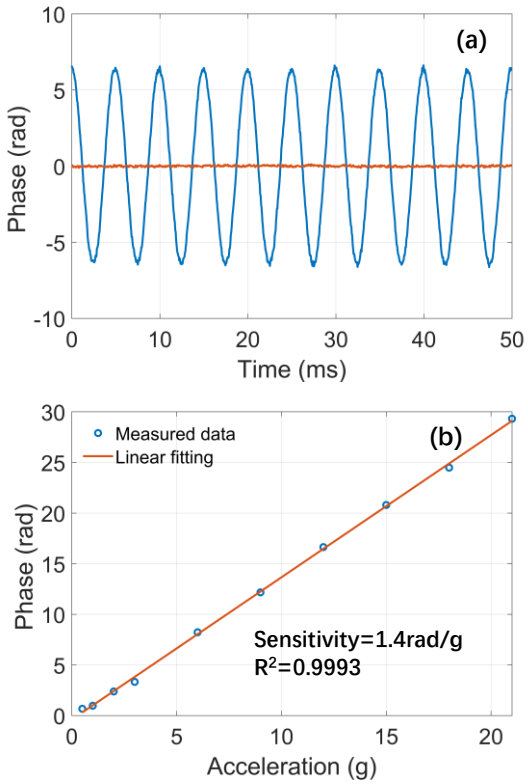

Fig. 5. (a) Measured sinusoidal vibration with acceleration of 9g at 200 Hz. The red line shows a reference phase at the end of FUT where vibration is not applied. (b) Output of optical fiber accelerometer as a function of acceleration. Red line is the linear curve fitting.

To fabricate the proposed accelerometer, a 2-m-long fiber is wrapped on the transducer cylinder. Fig. 5(a) shows the measured phase shift of the optical fiber accelerometer in the time domain with or without sinusoidal acceleration at 200 Hz. It can be seen that the vibration signal can be retrieved with high fidelity and the standard deviation of the phase signal without vibration is 0.04 rad. Fig. 5(b) illustrates the response of the accelerometer with different accelerations and the red line is the linear fitting result. The sensitivity is estimated to be 1.4 rad/g, while the coefficient of determination R^2 is 0.9993, indicating that a good linear relationship is achieved for vibration sensing. According to the simulation results and Equation (1), the length conversion coefficient η is estimated to 1.1%. The measurement error of our system is evaluated by using standard deviation of the noise signal and sensitivity, which is about 0.03 g. The sensitivity of the accelerometer is mainly determined by the inertial mass weight and the coiled fiber length. Inertial mass with a larger weight will increase the sensitivity. However, a tradeoff must be made between the acceleration sensitivity and the resonant frequency. An accelerometer with a higher sensitivity usually leads to a lower resonant frequency. As suggested by Equation (1), increasing the length of fiber coiled on the transducer will also increase the sensitivity. This is because the accumulated phase shift along a longer length of the coiled fiber will induce a larger phase difference between φ_{i+1} and φ_i.

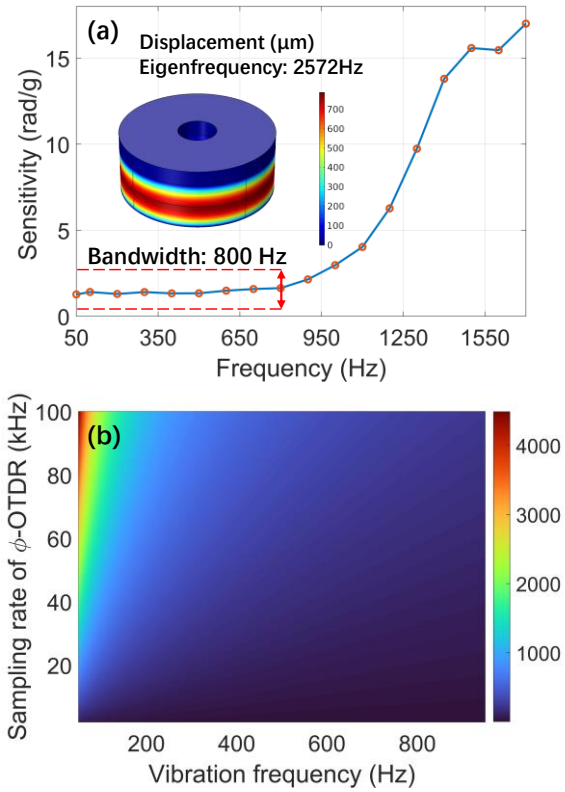

Fig. 6. (a) Frequency response characteristics of the accelerometer. Inset shows the simulated displacement at an eigenfrequency of 2572 Hz. (b) Theoretical maximum detectable acceleration with different vibration frequencies and sampling rate of DAS.

Furthermore, the frequency response of the accelerometer is characterized by increasing the frequencies of the acceleration from 50 Hz to 1700 Hz, as shown in Fig. 6(a). It can be seen that from 50 Hz to 800 Hz, the accelerometer shows a flat response with an average sensitivity of 1.42 rad/g, and the fluctuation is less than 9.1%. The sensitivity increases dramatically from 1000 Hz due to the excitation frequency approaching the natural frequency of the accelerometer. At 1700 Hz the sensitivity is about 17 rad/g, which is 10 times higher than that of the flat region. The resonant frequency of the proposed accelerometer is simulated by using finite element software, and the displacement at eigenfrequency is shown in Fig. 6(a) inset. The resonant frequency is expected to 2.5 kHz, which is not measured due to the limitation of our setup and the phase unwrapping algorithm. In IQ demodulation-based heterodyne detection DAS, the demodulated phase was wrapped between -π to π. To recover the phase using the unwrapping algorithm, phase change between adjacent points should be less than π rad. Therefore, the maximum detectable acceleration (MDA) depends on both the vibration frequency and the sampling rate of the DAS system, which is illustrated in Fig. 6(b). Based on the sensitivity of our accelerometer, the MDA is 4400 g when the vibration frequency and sampling rate of the DAS are 50 Hz and 100 kHz, respectively while the MDA decreases to 280 g with the vibration frequency being 800 Hz and sampling rate being 100 kHz.

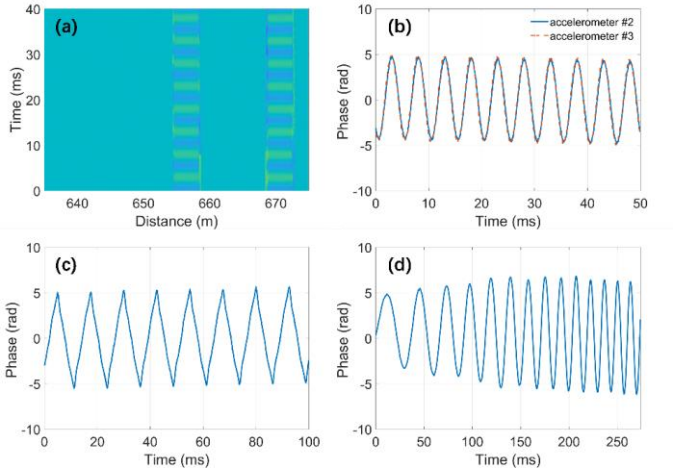

Fig. 7. (a) Measured quasi-distributed vibration signal of accelerometer #2 and #3. Retrieved time domain signal of (b) sinusoidal vibration, (c) triangular vibration, and (d) chirp vibration.

Quasi-distributed vibration sensing is also investigated. Both accelerometers #2 and #3 are fixed on the vibration exciter, different vibrations are generated to demonstrate the vibration recovery performance. First, a 200 Hz sinusoidal wave is measured, and the retrieved signal is shown in Fig. 7(a). The location and signal of two accelerometers can be clearly identified, and the time domain signal is shown in Fig. 7(b). Fig. 7(c) and Fig. 7(d) are the retrieved triangular wave and chirp wave, indicating that the quasi-distributed system is capable of high-fidelity waveform recovery with wide and flat frequency response. It should be noted that the bending radius of optical fiber is 2 cm, which is larger than the critical bending radius of single mode fiber at wavelength 1.5 μm (8 mm), enabling a low loss for the accelerometer. The total loss of an accelerometer is about 0.03 dB by employing an automated fiber optic winding

machine, thus the multiplexing number can expect to be several hundred.

To fairly compare the performance of UWFBG accelerometer #2 and SMF accelerometer #1, a 200 Hz sinusoidal wave is simultaneously applied to the accelerometers. The retrieved time domain signals by the two accelerometers are shown in Fig. 8(a). Fig. 8(b) is the calculated power spectrum densities (PSD) of the vibration signals in Fig. 8(a). It is obvious that the noise floor of the UWFBG accelerometer is lower than that of the SMF accelerometer, and the SNR of the vibration signal is enhanced by 10.3 dB.

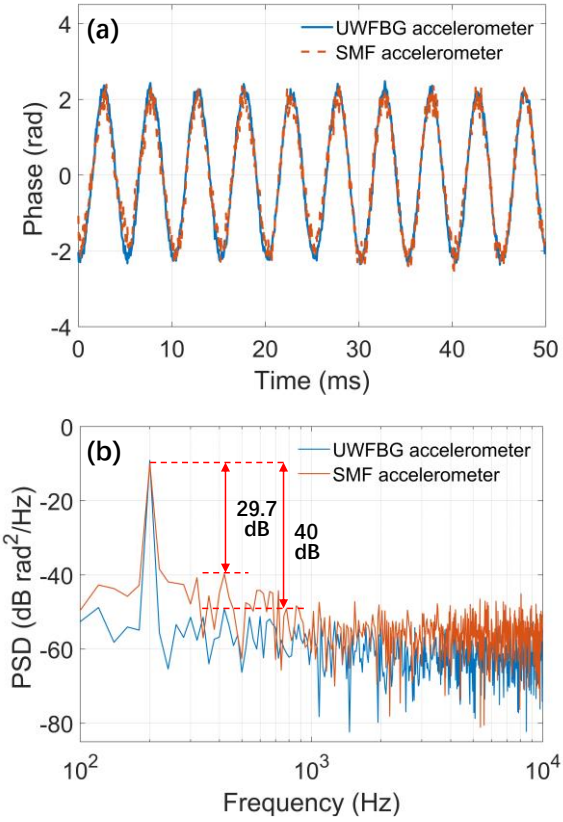

Fig. 8. (a) Retrieved time domain signals of UWFBG accelerometer #2 and SMF accelerometer #1, respectively. (b) PSDs (power spectrum density) of signal in (a).

In addition to having higher SNR due to the more stable and relatively stronger reflected light from the reflecting points in UWFBG, UWFBG accelerometer also avoids the coherent Rayleigh noise and therefore greatly suppresses fading probability. To quantitively analyze the influence of fading on the standard SMF accelerometer and UWFBG accelerometer, the fading probabilities are measured statistically. We acquired 2000 traces every second with a total acquisition time of 2000 seconds. Vibration is not applied to the accelerometers during the measurement. The histograms of the intensity (in dB scale) at SMF accelerometer #1 and UWFBG accelerometer #2 are drawn in Fig. 9(a). The histogram of SMF accelerometer #1 exhibits typical Rayleigh distribution with a peak located at -5.5 dB, while the peak of UWFBG accelerometer #2 is located at 5.2 dB. The cumulative distribution function (C.D.F.) is then calculated to characterize the corresponding histograms, as shown in Fig. 9(b). The C.D.F. curve of UWFBG accelerometer #2 is obviously right shifted with higher SNR. If the noise floor (i.e., -18.5 dB) is used as the threshold, the percentage of points below the threshold for the SMF accelerometer #1 is 0.3%. For UWFBG accelerometer #2, all points are well above the noise floor. The long-term statistical analysis verifies the effectiveness of the interference fading elimination of the accelerometer based on UWFBG. Next, SMF accelerometer #1 and UWFBG accelerometer #2 are put on the vibration shaker, where a 200 Hz sine wave is applied. Fig. 9(c) shows a typical interference fading that affected the demodulated vibration signal at SMF accelerometer #1. During the 20 ms vibration period, there are three moments that the amplitudes are below the noise floor, and the phase at the corresponding time cannot be successfully demodulated. However, the amplitudes of UWFBG accelerometer #2 are ~10 dB higher than that of SMF accelerometer #1, as shown in Fig. 9(d). Therefore, the phase can be successfully demodulated.

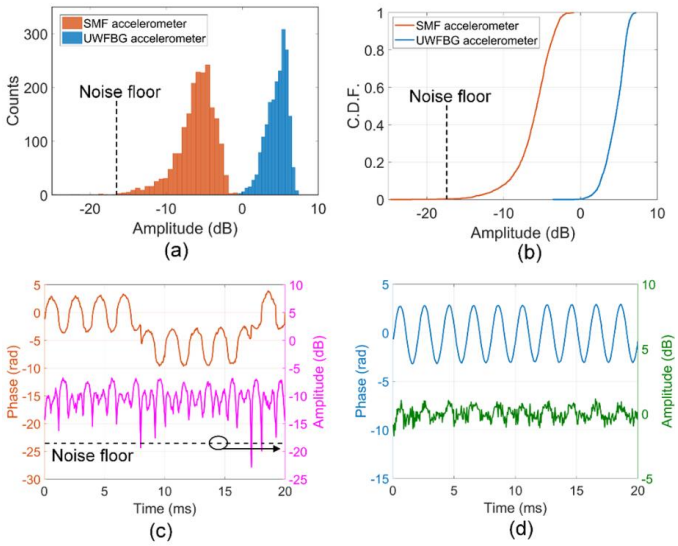

Fig. 9. (a) Histogram distributions of the amplitudes at SMF accelerometer #1 and UWFBG accelerometer #2; (b) corresponding cumulative distribution functions of SMF accelerometer and UWFBG accelerometer; (c) phase and amplitude of 200Hz vibration signal at SMF accelerometer #1; (d) phase and amplitude of 200Hz vibration signal at UWFBG accelerometer #2.

V. Conclusion

In summary, we have proposed a scheme of enhanced quasi-distributed accelerometer array based on φ-OTDR and ultra-weak fiber Bragg grating. A transducer cylinder was employed to transform the vertical acceleration to an axial strain and stress of the sensing fiber, thereby realizing high-fidelity vibration measurement. Meanwhile, an ultra-weak fiber Bragg grating (UWFBG) array that has relatively higher reflectivity and more stable reflection point was utilized to improve the SNR and eliminate Rayleigh fading. The experimental results have shown that acceleration sensing with an accuracy of 0.03 g and sensitivity of 1.4 rad/g could be achieved over 500 m UWFBG when the operating frequency was from 50 Hz to 800 Hz. Although only 3 accelerometers were multiplexed in this demonstration, hundreds of such accelerometers can be multiplexed along a single fiber since the loss for an accelerometer is about 0.03 dB. By employing an automated

fiber optic winding machine, the winding tension, the rotation angular velocity, and the length of fiber can be controlled precisely, making it possible to mass-produce accelerometers with good repeatability. The proposed sensing system offers high sensing sensitivity, large multiplexing capacity, and no interference fading and can be applied for structural health monitoring of large buildings and machinery.

REFERENCES

[1] N. Ahmad, R. A. R. Ghazilla, N. M. Khairi, and V. Kasi, "Reviews on various inertial measurement unit (IMU) sensor applications," *International Journal of Signal Processing Systems*, vol. 1, no. 2, pp. 256–262, 2013.

[2] D. K. Shaeffer, "MEMS inertial sensors: A tutorial overview," *IEEE Communications Magazine*, vol. 51, no. 4, pp. 100–109, 2013.

[3] N. El-Sheimy and A. Youssef, "Inertial sensors technologies for navigation applications: State of the art and future trends," *Satellite Navigation*, vol. 1, no. 1, pp. 1–21, 2020.

[4] F. A. Levinzon, "Fundamental noise limit of piezoelectric accelerometer," *IEEE Sensors Journal*, vol. 4, no. 1, pp. 108–111, 2004.

[5] A. Partridge *et al.*, "A high-performance planar piezoresistive accelerometer," *Journal of microelectromechanical systems*, vol. 9, no. 1, pp. 58–66, 2000.

[6] M. Benmessaoud and M. M. Nasreddine, "Optimization of MEMS capacitive accelerometer," *Microsystem Technologies*, vol. 19, no. 5, pp. 713–720, 2013.

[7] J. M. López-Higuera, L. R. Cobo, A. Q. Incera, and A. Cobo, "Fiber optic sensors in structural health monitoring," *Journal of lightwave technology*, vol. 29, no. 4, pp. 587–608, 2011.

[8] F. Marignetti *et al.*, "Fiber Bragg grating sensor for electric field measurement in the end windings of high-voltage electric machines," *IEEE Transactions on Industrial Electronics*, vol. 63, no. 5, pp. 2796–2802, 2016.

[9] X. Wang, Y. Guo, L. Xiong, and H. Wu, "High-frequency optical fiber Bragg grating accelerometer," *IEEE Sensors journal*, vol. 18, no. 12, pp. 4954–4960, 2018.

[10] O. P. Parida, J. Nayak, and S. Asokan, "Design and validation of a novel high sensitivity self-temperature compensated fiber Bragg grating accelerometer," *IEEE Sensors Journal*, vol. 19, no. 15, pp. 6197–6204, 2019.

[11] F. Zhang, S. Jiang, C. Wang, J. Ni, and Q. Zhao, "Broadband and high sensitivity FBG accelerometer based on double diaphragms and h-shaped hinges," *IEEE Sensors Journal*, vol. 21, no. 1, pp. 353–359, 2020.

[12] A. Stefani, S. Andresen, W. Yuan, N. Herholdt-Rasmussen, and O. Bang, "High sensitivity polymer optical fiber-Bragg-grating-based accelerometer," *IEEE Photonics Technology Letters*, vol. 24, no. 9, pp. 763–765, 2012.

[13] C. Chen, D. Zhang, G. Ding, and Y. Cui, "Broadband Michelson fiber-optic accelerometer," *Applied optics*, vol. 38, no. 4, pp. 628–630, 1999.

[14] R. Pechstedt and D. Jackson, "Performance analysis of a fiber optic accelerometer based on a compliant cylinder design," *Review of scientific instruments*, vol. 66, no. 1, pp. 207–214, 1995.

[15] Z. Zhao, Z. Yu, K. Chen, and Q. Yu, "A fiber-optic Fabry-Perot accelerometer based on high-speed white light interferometry demodulation," *Journal of Lightwave Technology*, vol. 36, no. 9, pp. 1562–1567, 2018.

[16] G. Zhang *et al.*, "Fiber optic birefringence enhanced accelerometer based on polarized modal interferometer," *Optics Communications*, vol. 442, pp. 8–12, 2019.

[17] Z. Liu *et al.*, "Novel accelerometer realized by a polarization-maintaining photonic crystal fiber for railway monitoring applications," *Optics express*, vol. 27, no. 15, pp. 21597–21607, 2019.

[18] L. Htein, D. S. Gunawardena, W.-H. Chung, H.-Y. Au, and H.-Y. Tam, "Accelerometer employing a side-hole fiber in a Sagnac interferometer," *Journal of Lightwave Technology*, vol. 39, no. 10, pp. 3303–3311, 2021.

[19] H. Li *et al.*, "Ultra-high sensitive quasi-distributed acoustic sensor based on coherent OTDR and cylindrical transducer," *Journal of Lightwave Technology*, vol. 38, no. 4, pp. 929–938, 2019.

[20] Z. Sha, H. Feng, and Z. Zeng, "Phase demodulation method in phase-sensitive OTDR without coherent detection," *Optics Express*, vol. 25, no. 5, pp. 4831–4844, 2017.

[21] J. Pastor-Graells, H. F. Martins, A. Garcia-Ruiz, S. Martin-Lopez, and M. Gonzalez-Herraez, "Single-shot distributed temperature and strain tracking using direct detection phase-sensitive OTDR with chirped pulses," *Optics express*, vol. 24, no. 12, pp. 13121–13133, 2016.

[22] Y. Shan *et al.*, "An enhanced distributed acoustic sensor based on UWFBG and self-heterodyne detection," *Journal of Lightwave Technology*, vol. 37, no. 11, pp. 2700–2705, 2019.

[23] Y. Wang, H. Zheng, and C. Lu, "High-sensitivity distributed relative salinity sensor based on frequency-scanning φ-OTDR," *Optics Express*, vol. 30, no. 13, pp. 22860–22870, 2022.

[24] D. Chen, Q. Liu, and Z. He, "Phase-detection distributed fiber-optic vibration sensor without fading-noise based on time-gated digital OFDR," *Optics express*, vol. 25, no. 7, pp. 8315–8325, 2017.

[25] J. Jiang, Z. Wang, Z. Wang, Z. Qiu, C. Liu, and Y. Rao, "Continuous chirped-wave phase-sensitive optical time domain reflectometry," *Optics Letters*, vol. 46, no. 3, pp. 685–688, 2021.

[26] Z. Zhao *et al.*, "Interference fading suppression in φ-OTDR using space-division multiplexed probes," *Optics Express*, vol. 29, no. 10, pp. 15452–15462, 2021.

[27] H. Wu, B. Zhou, K. Zhu, C. Shang, H.-Y. Tam, and C. Lu, "Pattern recognition in distributed fiber-optic acoustic sensor using an intensity and phase stacked convolutional neural network with data augmentation," *Optics Express*, vol. 29, no. 3, pp. 3269–3283, 2021.

[28] K. Zhu *et al.*, "Multipath distributed acoustic sensing system based on phase-sensitive optical time-domain reflectometry with frequency division multiplexing technique," *Optics and Lasers in Engineering*, vol. 142, p. 106593, 2021.

[29] X. He, M. Zhang, S. Xie, F. Liu, L. Gu, and D. Yi, "Self-referenced accelerometer array multiplexed on a single fiber using a dual-pulse heterodyne phase-sensitive OTDR," *Journal of lightwave technology*, vol. 36, no. 14, pp. 2973–2979, 2018.

[30] P. S. Westbrook *et al.*, "Enhanced optical fiber for distributed acoustic sensing beyond the limits of Rayleigh backscattering," *IScience*, vol. 23, no. 6, p. 101137, 2020.